View metadata, citation and similar papers at core.ac.uk

brought to you by CORE

provided by Boise State University - ScholarWorks

Boise State University
ScholarWorks

Materials Science and Engineering Faculty Publications and Presentations

Department of Materials Science and Engineering

10-11-2013

High Field Breakdown Characteristics of Carbon Nanotube Thin Film Transistors

Man Prakash Gupta
Georgia Institute of Technology

Ashkan Behnam
University of Illinois at Urbana-Champaign

Feifei Lian
University of Illinois at Urbana-Champaign

David Estrada
Boise State University

Eric Pop
University of Illinois at Urbana-Champaign

See next page for additional authors

This is an author-created, un-copyedited version of an article accepted for publication in *Nanotechnology.* IOP Publishing Ltd is not responsible for any errors or omissions in this version of the manuscript or any version derived from it. The definitive publisher-authenticated version is available online at DOI: 10.1088/0957-4484/24/40/405204.

Authors
Man Prakash Gupta, Ashkan Behnam, Feifei Lian, David Estrada, Eric Pop, and Satish Kumar

This article is available at ScholarWorks: http://scholarworks.boisestate.edu/mse_facpubs/169

This is an author-produced, peer-reviewed version of this article. The final, definitive version of this document can be found online at *Nanotechnology*, published by Institute of Physics. Copyright restrictions may apply. DOI: 10.1088/0957-4484/24/40/405204.

High Field Characteristics of Carbon Nanotube Thin Film Transistors

Man Prakash Gupta
G. W. Woodruff School of Mechanical Engineering
Georgia Institute of Technology
Atlanta, GA 30332, USA

Ashkan Behnam
Micro & Nanotechnology Laboratory, and
Dept. of Electrical & Computer Eng.
University of Illinois at Urbana-Champaign
Urbana, IL 61801, USA

Feifei Lian
Micro & Nanotechnology Laboratory, and
Dept. of Electrical & Computer Eng.
University of Illinois at Urbana-Champaign
Urbana, IL 61801, USA

David Estrada
Micro & Nanotechnology Laboratory, and
Dept. of Electrical & Computer Eng.
University of Illinois at Urbana-Champaign
Urbana, IL 61801, USA

Eric Pop
Micro & Nanotechnology Laboratory, and
Dept. of Electrical & Computer Eng.
University of Illinois at Urbana-Champaign
Urbana, IL 61801, USA

and

Beckman Institute for Advanced Science and Technology
University of Illinois at Urbana-Champaign
Urbana, IL 61801, USA

Satish Kumar
G. W. Woodruff School of Mechanical Engineering
Georgia Institute of Technology
Atlanta, GA 30332, USA

Email: Satish.kumar@me.gatech.edu

Abstract

The high-field properties of carbon nanotube (CNT) network thin film transistors (CN-TFTs) are important for their practical operation, and for understanding their reliability. Using a combination of experimental and computational techniques we show how the channel geometry (length L_C and width W_C) and network morphology (average CNT length L_t and alignment angle distribution θ) affect heat dissipation and high-field breakdown in such devices. The results suggest that when $W_C \geq L_t$, the breakdown voltage remains independent of W_C but varies linearly with L_C. The breakdown power varies almost linearly with both W_C and L_C when $W_C >> L_t$. We also find that the breakdown power is more susceptible to the variability in the network morphology compared to the breakdown voltage. The analysis offers new insight into the tunable heat dissipation and thermal reliability of CN-TFTs which can be significantly improved through optimization of the network morphology and device geometry.

1. Introduction

Carbon nanotubes (CNTs) are promising and useful materials for several applications due to their good thermal, electrical, optical and mechanical properties [1, 2]. Several studies have been performed in the past decade to explore and develop devices which could leverage the excellent properties of individual carbon nanotubes (CNTs) and their two- and three-dimensional (2D and 3D) networks [2-8]. In particular, CNT network thin film transistors (CN-TFTs) have been explored for a wide range of applications such as flexible displays, sensors, antennas, etc. [2, 4, 7-13]. Significant efforts have been made in recent years aimed at overcoming fabrication challenges to improve the performance of these devices [3, 14-19]. However, fewer studies have been focused on the heat dissipation in these devices, which is an important aspect of CN-TFT operation [20, 21]. CNT networks are typically supported on thermally insulating substrates such as glass or plastics, which have very low thermal conductivity and where the excessive self-heating in CN-TFTs under high field operations can lead to the breakdown of these devices [20, 21].

This is an author-produced, peer-reviewed version of this article. The final, definitive version of this document can be found online at *Nanotechnology*, published by Institute of Physics. Copyright restrictions may apply. DOI: 10.1088/0957-4484/24/40/405204.

CN-TFTs with a large aspect ratio [(channel length L_C / channel width W) ≫ 1] have been investigated previously to achieve higher ON/OFF current ratio. Narrow W_C and large L_C in CN-TFTs (Fig. 1) help in reducing the number of metallic percolating paths in unsorted CNT networks which typically have a 1:2 metallic (M) – semiconducting (S) ratio [3, 22]. However, such high aspect ratios can also lead to substantial variability and non-uniformity in the ON current [23]. In addition, a CNT network is comprised of individual single-walled CNTs (SWCNTs) of varying lengths (L_t) and alignment (θ) with respect to the source and drain electrodes. Previous studies have shown that the variability in the CNT network morphology can significantly affect the channel resistance and device performance [24, 25]. Therefore these variations in the channel geometry and network morphology are very likely to influence the reliability and breakdown behavior of CN-TFTs as well. The variation in the breakdown behavior for a given TFT geometry can lead to instability and/or unreliability during the operation of CN-TFTs. Thus, it is very important to understand how the geometrical parameters affect the high-field operation of the CN-TFT in order to optimize the device design for reliable and uniform behavior. While our previous work [26] has correlated the electronic properties of SWCNTs within a CN-TFT channel to the device thermal reliability, the effects of channel geometry and network morphology on CN-TFT power and reliability have not been studied in detail.

In this work, we apply both experimental and computational methods to understand the breakdown behavior and thermal reliability of CN-TFTs. We examine the breakdown characteristics such as peak power (or breakdown power, P_{BD}) and the corresponding source-to-drain voltage referred to as the breakdown voltage (V_{BD}) of CN-TFTs in order to find their relation with the aforementioned geometrical parameters. We first analyze the breakdown characteristics and their standard deviations for smaller and larger W_C at various L_C for random networks with constant CNT length, L_t. Next, we systematically vary the alignment of CNTs in the network for a given L_C, W_C and L_t to study the effect of network alignment on the breakdown behavior. Subsequently, we consider a general case employing different log-normal distributions of L_t in conjunction with several alignment distributions for a given L_C and W_C. The results suggest that when W_C is greater than the average L_t, V_{BD} remains independent of W_C and varies linearly with L_C. The variation in the distribution of alignment and L_t does not significantly affect V_{BD}. However, we find that P_{BD} increases with both L_C and W_C. In particular, for large W_C, P_{BD} varies linearly with both W_C and L_C. Our results suggest that the thermal reliability of CN-TFTs can be improved by optimizing the CNT length and alignment distribution. The analysis presented here, provides new insight into optimizing the device parameters in order to engineer thermal reliability and uniformity in CN-TFT performance characteristics.

2. Methodology

Carbon nanotubes synthesized by arc discharge method are used as starting materials for all the samples. The diluted solution containing SWCNTs and surfactant is vacuum filtered through a mixed cellulose ester membrane to form CNT network followed by rinsing with water to remove the residual surfactant. The network is then transferred to supporting substrates of SiO_2 (t_{ox} = 300 nm) on highly n-doped Si wafers (t_{Si} = 500 μm) with predefined electrical contacts and then the filter is dissolved [26]. The device channels are patterned by photolithography and/or electron beam lithography (for submicron width dimensions). The Si substrate acts as a back-gate, and unless otherwise noted we set the gate-to-source voltage (V_{GS} = -40 V) such that both M and S type CNTs in the network are in the "on" state (V_{GS} is significantly below the threshold voltage) while the source-to-drain voltage (V_{SD}) is increased until network breakdown. Device characterization and breakdown were conducted in air at room temperature ambient (T_0 = 25 °C).

For computational analysis, we employ a coupled electro-thermal model to analyze the current, power, and temperature distribution in the device [21, 22, 27, 28]. A brief description about the governing equations is provided below.

This is an author-produced, peer-reviewed version of this article. The final, definitive version of this document can be found online at *Nanotechnology*, published by Institute of Physics. Copyright restrictions may apply. DOI: 10.1088/0957-4484/24/40/405204.

2.1 Thermal Transport

The thermal transport in the device consisting of CNT-network, oxide layer and Si substrate is simulated using the diffusive energy transport equations, which can be written in the following non-dimensional form [28]:

$$\frac{d^2\xi_i}{ds^{*2}} + \tilde{G}_S\left(\xi_{\mathrm{OX}} - \xi_i\right) + \sum_{\substack{\text{intersecting} \\ \text{tubes j}}} \tilde{G}_C\left(\xi_j - \xi_i\right) + \frac{d}{L_t}\frac{q_i^{'}}{Q^{'}} = 0 \qquad (1)$$

$$\nabla^{*2}\xi_{\mathrm{OX}} + \sum_{i=1}^{N_{tubes}} \tilde{G}_S\gamma\left(\xi_i - \xi_{\mathrm{OX}}\right) = 0 \qquad (2)$$

$$\nabla^{*2}\xi_{\mathrm{Si}} = 0 \qquad (3)$$

Here, $\xi = (T-T_\infty)/(Q^{'}dL_t/k_t)$ is the non-dimensional form of temperature (T). T_∞ denotes the ambient temperature, $Q^{'}$ is a reference power per unit volume, d is the diameter of CNT, and k_t is the axial thermal conductivity of CNT. ξ_i, ξ_{OX} and ξ_{Si} are the non-dimensionalized temperatures of a section of the ith CNT, oxide, and Si, respectively. Asterisk symbol is used to refer to length variables which are non-dimensionalized by d. Equation (1) governs the temperature of any i^{th} CNT along its axial direction (length variable s); the second and third terms in this equation represent thermal interactions at CNT-oxide interface and at CNT-CNT junctions, respectively. $q_i^{'}$ is the volumetric Joule heating term within the CNT which is obtained from the solution of electrical transport equations (discussed below). $\tilde{G}_C$ and $\tilde{G}_S$ represent the non-dimensional thermal contact conductance at CNT-CNT junctions and CNT-oxide interface respectively and their estimated values are obtained from our previous work [21]. Equation (2) describes the temperature in the oxide layer and the second term in this equation represents CNT-oxide thermal interaction, which is summed over all the CNTs. The parameter γ in this term characterizes the contact geometry. Equation (3) describes the temperature of the Si layer.

We use a constant temperature boundary condition ($T = 298$ K) at the bottom surface of Si substrate, while a convective boundary condition [21, 28] is imposed at the top surface of the oxide layer. The lateral boundaries have been assumed to be thermally insulated. The boundary conditions have been selected to simulate the experimental conditions.

2.2 Electrical Transport

The electrical transport in the carbon nanotubes has been described by Poisson and current continuity equations as follows [13, 22, 28]:

$$\frac{d^2\psi_i}{ds^2} + \frac{\rho_i}{\varepsilon} - \frac{(\psi_i - V_G)}{\lambda^2} + \sum_{j\neq i}\frac{(\psi_j - \psi_i)}{\lambda_{ij}^2} = 0, \qquad (4)$$

$$\nabla.J_{pi} + \sum_{j\neq i} C_{ij}^{p}(p_j - p_i) = 0, \qquad (5)$$

$$\nabla.J_{ni} + \sum_{j\neq i} C_{ij}^{n}(n_j - n_i) = 0, \qquad (6)$$

Here, ψ is the electrostatic potential, V_G is the gate voltage, ρ is the net charge density, ε is the permittivity of CNT. The third term in Poisson equation represents the gating effect [28] with screening length, $\lambda = (\varepsilon_{CNT}\, t_{OX}\, d/\varepsilon_{OX})^{0.5}$. Here, ε_{CNT} and ε_{OX} are the dielectric constants for the CNT and gate oxide respectively and t_{OX} is the oxide thickness. The forth term in Equation (4) describes the inter-tube electrostatic interaction at CNT-CNT junctions with screening length, $\lambda \sim d$. Equations (5) and (6) are current continuity equations for holes and electrons respectively, where J is current density given by drift –diffusion equations. Hole and electron charge density are represented by p and n,

This is an author-produced, peer-reviewed version of this article. The final, definitive version of this document can be found online at *Nanotechnology*, published by Institute of Physics. Copyright restrictions may apply. DOI: 10.1088/0957-4484/24/40/405204.

respectively. The second term, $C_{ij}^{n}(n_j - n_i)$ or $C_{ij}^{p}(p_j - p_i)$, in the continuity equations represents charge (electrons or holes) transfer across the CNT-CNT junctions. The charge transfer coefficient ($C_{ij}^{n,p}$) is considered zero for *M-S* junctions to account for very low contact conductance compared to the *M-M* and *S*-S junctions [29]. The numerical values of major parameters in Equations (1-6) are provided in a separate table in the supplementary document. These electro-thermal equations are solved self-consistently to obtain the current, potential and temperature distribution in the CN-TFTs. Heterogeneous networks of *M* and *S* type CNTs (1:2 ratio) are considered in all simulations unless specified otherwise.

The model provides comprehensive details of the temperature and power distribution within the CNT network and thermal transport across substrate (Si) and insulator (SiO_2). Since these details are very difficult to obtain directly from the experiments, the model serves as an essential tool in analyzing the high-field transport and breakdown of CN-TFTs. The numerical model is validated by comparing the simulation results with the experimental data (see Section 3.1).

Under high field conditions, Joule heating can lead to oxidation of the CNTs in air if the temperature exceeds the breakdown temperature $T_{BD} \approx 600$ °C, resulting in the breakdown of the devices [20, 21, 30]. Thus, during this electrical breakdown process, the power dissipation in the device reaches a maximum value near T_{BD}, and then drops quickly to zero as the current paths within the network reform and oxidize, reaching catastrophic device failure. Back-gated device configuration has been selected for the experiments as it facilitates experimental measurements [20, 26]. All simulation results presented in this work are averaged over a large number of devices ($n \approx 100$) unless specified otherwise. Both mean as well as standard deviation of the breakdown characteristics are presented to understand the variability in the breakdown behavior for different device geometry and network morphology parameters.

3. Results and Discussion

3.1 Channel Geometry

We first analyze the effect of L_C and W_C on the breakdown characteristics. From the perspective of the device breakdown, the two important metrics are P_{BD} and V_{BD}. Fig. 2(a) shows the power dissipation in the device as a function of V_{SD} for three different cases of L_C = 5, 10, 15 μm at a network density of ρ = 15 CNTs/μm^2, W_C = 100 μm, and L_t = 2 μm. We find an excellent match between the experimental and simulation results. It should be noted that smaller L_C results in less resistance CNT networks which in turn leads to higher current (*i.e.*, higher power dissipation) at a given V_{SD}. This causes the device of smaller L_C to break earlier (*i.e.*, at a lower V_{SD}). V_{BD} and P_{BD} both linearly scale with L_C [Fig. 2(b) and 2(c)]. The error bars in these figures indicate the variation in breakdown characteristic of the random networks. The size of the error bar represents a 95 percent confidence interval for V_{BD} (or P_{BD}). The experimental values for both V_{BD} and P_{BD} fall well within the range of error bars estimated from the simulations. For a given network density, the number of percolating pathways decreases as L_C increases. As previously reported, [23] ON current shows greater variations when network density is decreased. Lowering the density is equivalent to reducing the number of percolating pathways, which also occurs when L_C is increased, and therefore the error bars increase as L_C increases. These results suggest that the variability in the breakdown for a given device geometry and network density can be substantial and require due consideration while predicting the device reliability [26].

Figure 3(a) shows the breakdown behavior of CN-TFTs for W_C = 4, 10, 20, 30, and 40 μm at L_C = 10 μm, L_t = 2 μm and ρ = 15 CNTs/μm^2. The curves in Fig. 3(a) resemble a 'bell' shape due to the statistical averaging. It can be observed that the V_{BD} does not change with W_C. Further, we find P_{BD} to be directly proportional to width when $W_C/L_t > 2$ [Fig. 3(b)]. We also note that the normalized standard deviation (σ_{norm}) of V_{BD} [Fig. 3(c)] and P_{BD} [Fig. 3(d)] increases when L_C is increased or W_C is decreased. For $W_C/L_t \leq 2$, we observe relatively large σ_{norm} due to significant incremental change in the number of percolating pathways [31]. We find that for ρ = 15 CNTs/μm^2, L_C = 10 μm and $W_C/L_t = 2$, less than 30% of the random networks out of 100 samples have a percolating path between source and drain. The probability of forming a percolating path further decreases as we increase L_C for $W_C/L_t \leq 2$. Therefore, we employ a denser network to study the breakdown behavior for $W_C/L_t \leq 2$.

This is an author-produced, peer-reviewed version of this article. The final, definitive version of this document can be found online at *Nanotechnology*, published by Institute of Physics. Copyright restrictions may apply. DOI: 10.1088/0957-4484/24/40/405204.

Figure 4 shows the dependence of breakdown behavior on L_C for narrow width devices (W_C/L_t = 0.75, 1, 1.5, 2) at ρ = 30 CNTs/μm^2. We find that V_{BD} is nearly invariant of the W_C for $W_C/L_t \geq 1$ [Fig. 4(a)]. P_{BD} follows width-dependent scaling with L_C such that higher width leads to greater change in P_{BD} per unit change in L_C [Fig. 4(b)]. A similar trend is observed in the experiments as shown in the Supplementary Information (Section S1). We note that σ_{norm} of V_{BD} [Fig. 4(c)] and P_{BD} [Fig. 4(d)] remain nearly invariant of L_C for $W_C/L_t \geq 1$ and σ_{norm} decreases as W_C increases at a given L_C. Overall, we note that larger values of L_C and W_C correspond to better device reliability as they lead to larger V_{BD}, greater P_{BD}, and better uniformity in device characteristics.

Previous studies [20, 21, 26, 32] on the CN-TFT breakdown show that the network breaks along a zigzag pattern across the channel when W_C is much greater than L_t. In the current study, we examine this breakdown pattern in CN-TFTs when W_C is comparable to L_t. Scanning electron microscopy (SEM) images from the experiments show that the breakdown pattern remains zigzag when L_C is small (few microns) for different values of W_C, as shown in Fig. 5 (a, d, g). Also, the length (L_{BD}) of the breakdown gap region [shown in Fig. 5(g)] is observed to be less than the average L_t which indicates a highly localized burning of CNTs. Further, L_{BD} increases as L_C is increased for a given W_C but does not change much with respect to W_C for a given L_C (Fig. 5). This trend underlines the role of temperature profile before the breakdown and electrostatic effects of the broken CNTs during the breakdown process. For devices with larger L_C, the temperature profile is more flat away from the contacts which leads to larger L_{BD}. In addition, higher electrostatic effect from the broken tubes amounts to greater induced electric field in the unbroken neighboring CNTs. This electrostatic effect is proportional to the applied voltage between source and drain at the breakdown (*i.e.,* V_{BD}) [32]. As V_{BD} linearly increases with L_C, the breakdown gap also follows nearly the same trend.

3.2 Network Morphology

3.2.1 Variable alignment angle with constant CNT length

In order to investigate the effect of CNT alignment on TFT breakdown behavior, we consider several alignment distributions of CNTs in the network. We define average alignment (θ_{avg}) such that for a specific value of θ_{avg}, a CNT in the network is allowed to make any angle between -2θ_{avg} and 2θ_{avg} with equal probability, as shown in Fig. 6.

Figure 7(a) shows a plot of power dissipation versus V_{SD} for different network alignments (from θ_{avg} = 9°- 45°). It is observed that for a highly aligned network (θ_{avg} < 10°), devices show negligible current due to the reduced number of percolating pathways bridging the source and drain contacts. However, as we increase θ_{avg}, the current increases due to the increasing number of percolating pathways. Previous studies [22] have also suggested that the ON current depends on the alignment and it reaches a maximum at θ_{avg} ~ 30° which is consistent with our results for V_{SD} < 20 V, as shown in Fig. 7(a). For the breakdown behavior analysis, we analyze P_{BD} and V_{BD} dependence on θ_{avg}. We find that the V_{BD} first decreases sharply and then shows a zigzag pattern with increasing θ_{avg}. Two local minima are observed at θ_{avg} = 22° and θ_{avg} = 36° [Fig. 7(b)]. V_{BD} lies in the small range of 26 V to 29 V for θ_{avg} > 10° which suggests a weak dependence of V_{BD} on alignment. The P_{BD} increases linearly as we increase θ_{avg} up to 27° and two 'local' maxima are observed at θ_{avg} = 27° and θ_{avg} = 40° [Fig. 7(c)].

In order to explore the nature of this dependence, we examine the breakdown pattern of the CNT networks. It should be noted that we consider the network to be composed of *M* and *S* type CNTs in 1:2 ratio. A Schottky barrier has been assumed to be present between metallic and semiconducting CNTs, and *M-S* junctions are considered to be electrically insulating since *M-M* or *S-S* junction conductance can be 2 orders of magnitude higher than *M-S* junction conductance [29]. We also showed in our previous work [21] that in general heat transfer across the CNT junctions is negligible in comparison to heat transfer across CNT-SiO_2 interface. Therefore the poor thermal contact conductance between CNTs makes crossed-CNT contacts thermally insulating as well [21]. This implies that the network can be considered to be composed of two independent 'parallel' networks of different densities and conductivities. Therefore the breakdown behavior and characteristics discussed are due to the combined breakdown behavior of pure metallic and semiconducting networks. Figure 8(a) shows a plot of power dissipation versus V_{SD} for different θ_{avg} at ρ = 15 CNTs/μm^2 of a homogeneous network (semiconducting CNTs only). We find that V_{BD} and P_{BD} exhibit only one minima (θ_{avg} = 20°) and maxima (θ_{avg} = 36°) respectively [Fig. 8(b) and (c)]. A similar trend is observed for pure metallic CNT networks. It should be noted, however, that the density of the metallic and semiconducting networks is in a 1:2 ratio within the combined network, and the location of maxima or minima of the breakdown characteristics depends on ρ [Fig. 9(a) and (b)]. This is responsible for the existence of the two local optimum points in breakdown characteristics of the heterogeneous network.

This is an author-produced, peer-reviewed version of this article. The final, definitive version of this document can be found online at *Nanotechnology*, published by Institute of Physics. Copyright restrictions may apply. DOI: 10.1088/0957-4484/24/40/405204.

3.2.2 Variable alignment angle with lognormal distribution of CNT length

We previously discussed the dependence of breakdown behavior on alignment of CNTs where L_t was kept constant. In this section, we study the breakdown behavior for a more general case where both CNT length and alignment are varied according to their respective distributions. Figure 10 illustrates the log normal distribution of L_t in the network. Here, the device size is $L_C \times W_C = 5 \times 5$ µm, and $\rho = 15$ CNTs/µm^2. All CNTs are considered to be semiconducting to analyze only the effects of length and alignment distributions. We consider three different cases of log-normal length distributions (average L_t, $\langle L_t \rangle = 1$ µm, 1.15 µm and 1.3 µm) and 9 cases of alignment distributions (range of $\theta_{avg} = 9°$ (highly aligned network) to 45° (random network)). The log-normal distribution is given by following equation:

$$f(L_t, \mu, \sigma) = \frac{1}{L_t \sigma \sqrt{2\pi}} \exp\left[-\frac{(\ln L_t - \mu)^2}{2\sigma^2} \right] \quad (7)$$

where f is the probability distribution function, L_t is the CNT length, μ is the mean and σ is the standard deviation of the CNT length. It should be noted that the lognormal distribution of CNT length has a practical significance as this distribution is typically observed in the experiments [26, 33]. We expect the log-normal distribution to affect the reliability and breakdown characteristics of homogenous CNT networks, as a previous study [25] reported that the resistivity of heterogeneous networks varies with the change in the parameters of the log-normal distribution.

Results (Fig. 11) suggest that the effect of the alignment on the breakdown behavior strongly depends on L_t distribution. We find that a L_t distribution with higher $\langle L_t \rangle$ provides higher P_{BD}. Also, the θ_{avg} corresponding to the maximum P_{BD} decreases when $\langle L_t \rangle$ is increased. In other words, better thermal reliability can be obtained when $\langle L_t \rangle$ is higher and the network is partially aligned. Interestingly, V_{BD} does not show much variation despite the fact that P_{BD} changes significantly. The trend of P_{BD} can be explained on the basis of the trade-off associated with the number of percolating paths and resistance of these paths. At lower θ_{avg}, the number of percolating paths in the channel will be less, but the resistance of these pathways will be also low due to the lower number of CNT junctions in these pathways. For higher values of θ_{avg}, the network tends toward a random distribution and the number of connections in the network increases, i.e., the number of effective percolative pathways increases, but the CNT junction density per pathway also increases. Therefore a maximum current (or power) should be achieved for some intermediate θ_{avg} which offers optimal channel resistance. As mentioned earlier, this optimal value of θ_{avg} decreases as $\langle L_t \rangle$ increases. We also note that the standard deviation in V_{BD} and P_{BD} shows little variation with change in $\langle L_t \rangle$ and θ_{avg}. However, the normalized value of it (σ_{norm}) changes due to the variation in the mean values of the respective variables [Fig. 12(a) and (b)]. More details about power variation with V_{SD} have been included in the Supplementary Information (Section S2).

4. Conclusion

In summary, we have studied the effects of channel geometry and network morphology on the high field breakdown of carbon nanotube network thin film transistors (CN-TFTs). We apply both experimental and computational techniques to examine the heat dissipation in the device and provide an in-depth analysis of two important characteristics (P_{BD} and V_{BD}) relevant to the breakdown process in CN-TFTs. We observe that the breakdown characteristics vary significantly with the channel length, but their dependence on the channel width is relatively very small. In a heterogeneous network, the breakdown characteristics and their relation with the network morphology vary with the ratio of metallic and semiconducting CNTs in the network. The analysis on breakdown behavior of CN-TFT for various log-normal CNT length distribution and several alignment distributions suggests that the heat dissipation and thermal reliability of CN-TFTs can be significantly improved by optimizing the network morphology parameters.

This is an author-produced, peer-reviewed version of this article. The final, definitive version of this document can be found online at *Nanotechnology*, published by Institute of Physics. Copyright restrictions may apply. DOI: 10.1088/0957-4484/24/40/405204.

Acknowledgement

Work at the University of Illinois Urbana-Champaign was sponsored in part by the National Science Foundation (NSF) CAREER grant ECCS 0954423 (E.P.), the NSF Graduate Research Fellowship (D.E.), and the Office of Naval Research (ONR) grant N00014-10-1-0853 (A.B.). M.P.G. acknowledges support from NSF grant ECCS-1028569. The authors thank Mark C. Hersam, Vinod Sangwan and Deep Jariwala for providing CNT networks and Edmond Chow for electron-beam (e-beam) lithography.

Supplementary Material

Supplementary material (additional results related to experimental breakdown characteristics and power-voltage curves for lognormal CNT length distributions) is available in the online version of this article.

References

[1] Reuss R H, Chalamala B R, Moussessian A, Kane M G, Kumar A, Zhang D C, Rogers J A, Hatalis M, Temple D, Moddel G, Eliasson B J, Estes M J, Kunze J, Handy E S, Harmon E S, Salzman D B, Woodall J M, Alam M A, Murthy J Y, Jacobsen S C, Olivier M, Markus D, Campbell P M and Snow E 2005 Macroelectronics: Perspectives on Technology and Applications *Proc. IEEE* **93** 1239-56

[2] Cao Q and Rogers J A 2009 Ultrathin Films of Single-Walled Carbon Nanotubes for Electronics and Sensors: A Review of Fundamental and Applied Aspects *Adv. Mater.* **21** 29-53

[3] Ha M, Xia Y, Green A A, Zhang W, Renn M J, Kim C H, Hersam M C and Frisbie C D 2010 Printed, Sub-3V Digital Circuits on Plastic from Aqueous Carbon Nanotube Inks *ACS Nano* **4** 4388-95

[4] Hu L, Hecht D S and Grüner G 2010 Carbon Nanotube Thin Films: Fabrication, Properties, and Applications *Chem. Rev.* **110** 5790-844

[5] Kocabas C, Pimparkar N, Yesilyurt O, Kang S J, Alam M A and Rogers J A 2007 Experimental and Theoretical Studies of Transport through Large Scale, Partially Aligned Arrays of Single-Walled Carbon Nanotubes in Thin Film Type Transistors *Nano Lett.* **7** 1195-202

[6] Schymura S, Kühnast M, Lutz V, Jagiella S, Dettlaff-Weglikowska U, Roth S, Giesselmann F, Tschierske C, Scalia G and Lagerwall J 2010 Towards Efficient Dispersion of Carbon Nanotubes in Thermotropic Liquid Crystals *Adv. Funct. Mater.* **20** 3350-7

[7] Wang C, Takei K, Takahashi T and Javey A 2013 Carbon nanotube electronics - moving forward *Chem. Soc. Rev.* **42** 2592-609

[8] Park S, Vosguerichian M and Bao Z 2013 A review of fabrication and applications of carbon nanotube film-based flexible electronics *Nanoscale* **5** 1727-52

[9] Okuda S, Okamoto S, Ohno Y, Maehashi K, Inoue K and Matsumoto K 2012 Horizontally Aligned Carbon Nanotubes on a Quartz Substrate for Chemical and Biological Sensing *J. Phys. Chem. C* **116** 19490-5

[10] Alizadegan R, Liao A, Xiong F, Pop E and Hsia K 2012 Effects of tip-nanotube interactions on atomic force microscopy imaging of carbon nanotubes *Nano Res.* **5** 235-47

[11] Sun D-m, Timmermans M Y, Tian Y, Nasibulin A G, Kauppinen E I, Kishimoto S, Mizutani T and Ohno Y 2011 Flexible high-performance carbon nanotube integrated circuits *Nat. Nano.* **6** 6

[12] Kumar S, Murthy J Y and Alam M A 2005 Percolating Conduction in Finite Nanotube Networks *Phys. Rev. Lett.* **95** 066802

[13] Kumar S, Pimparkar N, Murthy J Y and Alam M A 2006 Theory of transfer characteristics of nanotube network transistors *Appl. Phys. Lett.* **88** 123505

[14] Cao Q, Hur S H, Zhu Z T, Sun Y G, Wang C J, Meitl M A, Shim M and Rogers J A 2006 Highly Bendable, Transparent Thin-Film Transistors That Use Carbon-Nanotube-Based Conductors and Semiconductors with Elastomeric Dielectrics *Adv. Mater.* **18** 304-9

[15] Cao Q, Kim H-s, Pimparkar N, Kulkarni J P, Wang C, Shim M, Roy K, Alam M A and Rogers J A 2008 Medium-scale carbon nanotube thin-film integrated circuits on flexible plastic substrates *Nature* **454** 495-500

[16] Wang C, Zhang J, Ryu K, Badmaev A, De Arco L G and Zhou C 2009 Wafer-Scale Fabrication of Separated Carbon Nanotube Thin-Film Transistors for Display Applications *Nano Lett.* **9** 4285-91

[17] Arnold M S, Green A A, Hulvat J F, Stupp S I and Hersam M C 2006 Sorting carbon nanotubes by electronic structure using density differentiation *Nat. Nano.* **1** 6

This is an author-produced, peer-reviewed version of this article. The final, definitive version of this document can be found online at *Nanotechnology*, published by Institute of Physics. Copyright restrictions may apply. DOI: 10.1088/0957-4484/24/40/405204.

[18] Cao Q, Han S-j, Tulevski G S, Zhu Y, Lu D D and Haensch W 2013 Arrays of single-walled carbon nanotubes with full surface coverage for high-performance electronics *Nat. Nano.* **8** 180-6

[19] Sun D-m, Timmermans M Y, Tian Y, Nasibulin A G, Kauppinen E I, Kishimoto S, Mizutani T and Ohno Y 2011 Flexible high-performance carbon nanotube integrated circuits *Nat. Nano.* **6** 156-61

[20] Estrada D and Pop E 2011 Imaging Dissipation and Hot Spots in Carbon Nanotube Network Transistors *Appl. Phys. Lett.* **98** 073102

[21] Gupta M P, Chen L, Estrada D, Behnam A, Pop E and Kumar S 2012 Impact of thermal boundary conductances on power dissipation and electrical breakdown of carbon nanotube network transistors *J. Appl. Phys.* **112** 124506

[22] Pimparkar N, Cao Q, Kumar S, Murthy J Y, Rogers J and Alam M A 2007 Current and Voltage Characteristics of Long-Channel Nanobundle Thin-Film Transistors: "Bottom-Up" Perspective *IEEE Electron Device Lett.* **28** 157-60

[23] Pimparkar N, Cao Q, Rogers J and Alam M 2009 Theory and practice of “Striping” for improved ON/OFF Ratio in carbon nanonet thin film transistors *Nano Res.* **2** 167-75

[24] Timmermans M, Estrada D, Nasibulin A, Wood J, Behnam A, Sun D-m, Ohno Y, Lyding J, Hassanien A, Pop E and Kauppinen E 2012 Effect of carbon nanotube network morphology on thin film transistor performance *Nano Res.* **5** 307-19

[25] Hicks J, Behnam A and Ural A 2009 Resistivity in percolation networks of one-dimensional elements with a length distribution *Phys. Rev. E* **79** 012102

[26] Behnam A, Sangwan V K, Zhong X, Lian F, Estrada D, Jariwala D, Hoag A J, Lauhon L J, Marks T J, Hersam M C and Pop E 2013 High-Field Transport and Thermal Reliability of Sorted Carbon Nanotube Network Devices *ACS Nano* **7** 482

[27] Kumar S, Alam M A and Murthy J Y 2007 Computational Model for Transport in Nanotube-Based Composites With Applications to Flexible Electronics *J. Heat Transfer* **129** 500-8

[28] Kumar S, Pimparkar N, Murthy J Y and Alam M A 2011 Self-Consistent Electrothermal Analysis of Nanotube Network Transistors *J. Appl. Phys.* **109** 014315

[29] Fuhrer M S, Nygård J, Shih L, Forero M, Yoon Y-G, Mazzoni M S C, Choi H J, Ihm J, Louie S G, Zettl A and McEuen P L 2000 Crossed Nanotube Junctions *Science* **288** 494-7

[30] Hata K, Futaba D N, Mizuno K, Namai T, Yumura M and Iijima S 2004 Water-Assisted Highly Efficient Synthesis of Impurity-Free Single-Walled Carbon Nanotubes *Science* **306** 1362-4

[31] Li J and Zhang S-L 2009 Finite-size scaling in stick percolation *Phys. Rev. E* **80** 040104

[32] Shekhar S, Erementchouk M, Leuenberger M N and Khondaker S I 2011 Correlated electrical breakdown in arrays of high density aligned carbon nanotubes *Appl. Phys. Lett.* **98** 243121

[33] Sangwan V K, Ortiz R P, Alaboson J M P, Emery J D, Bedzyk M J, Lauhon L J, Marks T J and Hersam M C 2012 Fundamental Performance Limits of Carbon Nanotube Thin-Film Transistors Achieved Using Hybrid Molecular Dielectrics *ACS Nano* **6** 7480-8

This is an author-produced, peer-reviewed version of this article. The final, definitive version of this document can be found online at *Nanotechnology*, published by Institute of Physics. Copyright restrictions may apply. DOI: 10.1088/0957-4484/24/40/405204.

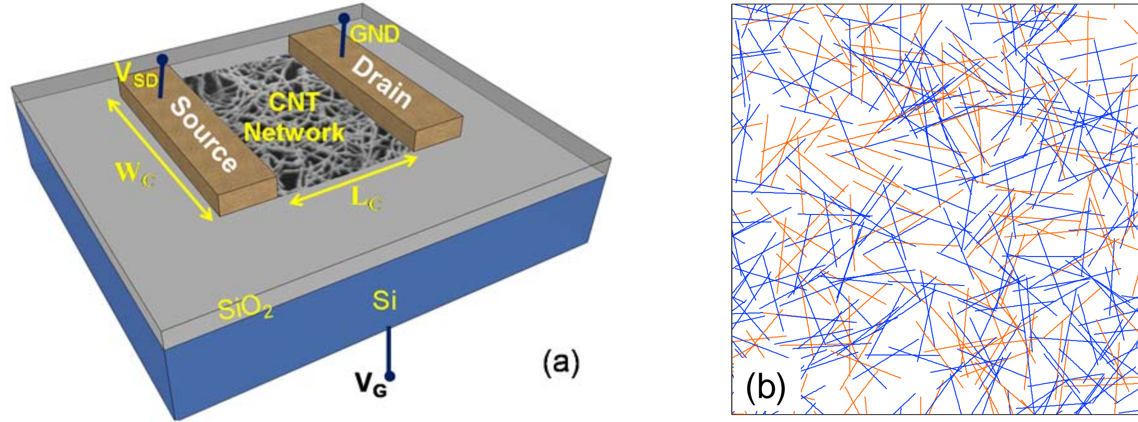

Figure 1. Schematic of (a) back-gated CN-TFT device with channel length (Lc) and channel width (W_C) similar to the devices experimentally tested. (b) A sample of simulated random network of CNTs; blue color is used for semiconducting and red for metallic CNTs.

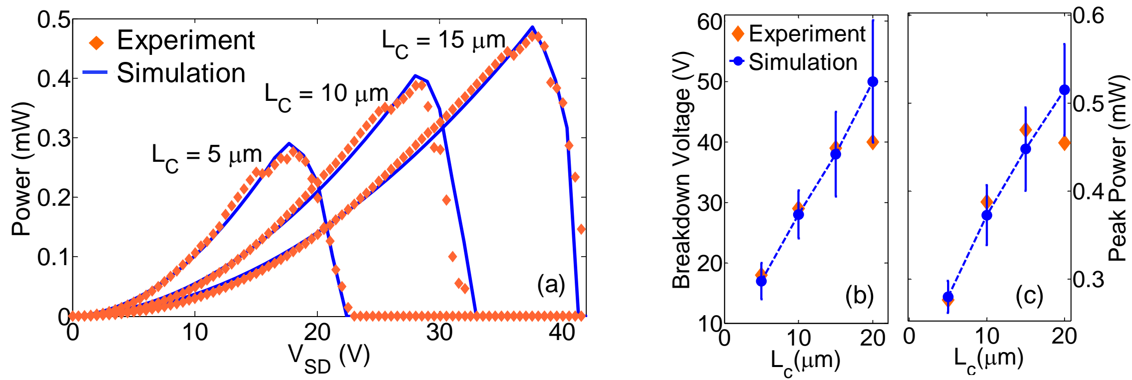

Figure 2. (a) Measured and simulated power dissipation in a CNT network versus source-to-drain voltage (V_{SD}) for three different channel lengths (L_C = 5, 10, 15 μm). Simulation results are presented for individual devices here. For a given L_C, power reaches a peak value and then drops quickly to zero as the CNT network breaks down due to the excessive Joule heating and CNT oxidation in air. The value of V_{SD} corresponding to the peak power (P_{BD}) is referred to as the breakdown voltage, V_{BD}. (b) V_{BD} versus L_C, and (c) P_{BD} versus L_C. The error bar represents a 95 percent confidence interval. The device is in the ON state at gate voltage V_{GS} = -40V. Device width W_C = 100 μm; CNT length L_t = 2 μm, network density ρ = 15 CNTs/μm^2. (b) and (c) contain simulation results which are averaged over 100 devices.

This is an author-produced, peer-reviewed version of this article. The final, definitive version of this document can be found online at *Nanotechnology*, published by Institute of Physics. Copyright restrictions may apply. DOI: 10.1088/0957-4484/24/40/405204.

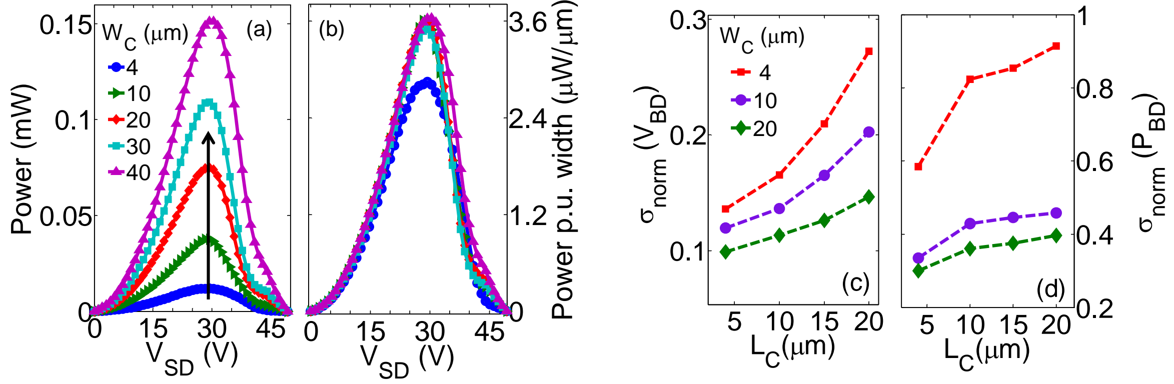

Figure 3. Numerical results for (a) power vs. V_{SD} (arrow indicates the increasing channel width), (b) power per unit width vs. V_{SD} for several channel widths (W_C = 4, 10, 20, 30, 40 μm); channel length, L_C = 10 μm, and network density, ρ = 30 CNTs/μm^2. Note that power per unit width becomes invariant with respect to W_C for sufficiently high W_C. (c) σ_{norm} of breakdown voltage (V_{BD}) vs. L_C, and (d) σ_{norm} of peak power (P_{BD}) vs. L_C. Here σ_{norm} = standard deviation / mean.

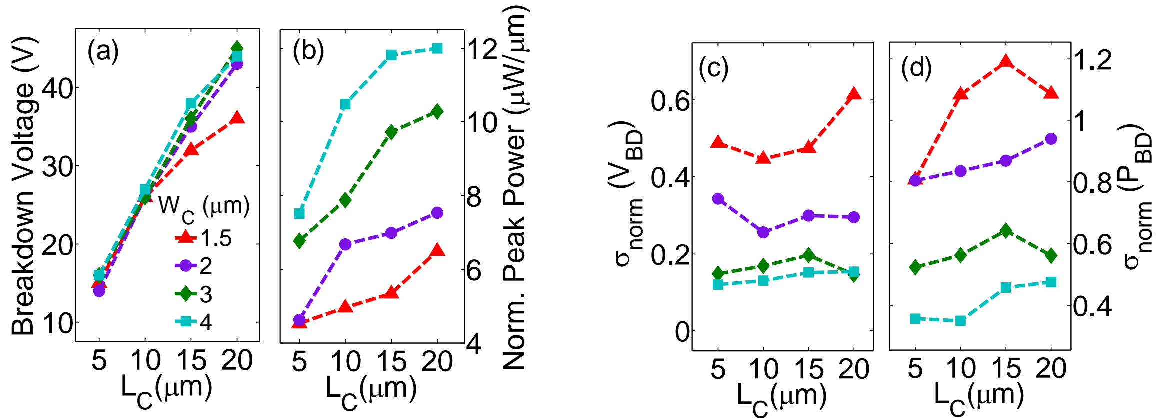

Figure 4. Numerical results for (a) breakdown voltage (V_{BD}) and (b) normalized peak power (with respect to W_C) in the CNT network vs. channel length (L_C) for smaller channel widths (W_C). (c) σ_{norm} of V_{BD}, (d) Peak power (PP) vs. L_C. Here, network density ρ = 30 CNTs/μm^2.

This is an author-produced, peer-reviewed version of this article. The final, definitive version of this document can be found online at *Nanotechnology*, published by Institute of Physics. Copyright restrictions may apply. DOI: 10.1088/0957-4484/24/40/405204.

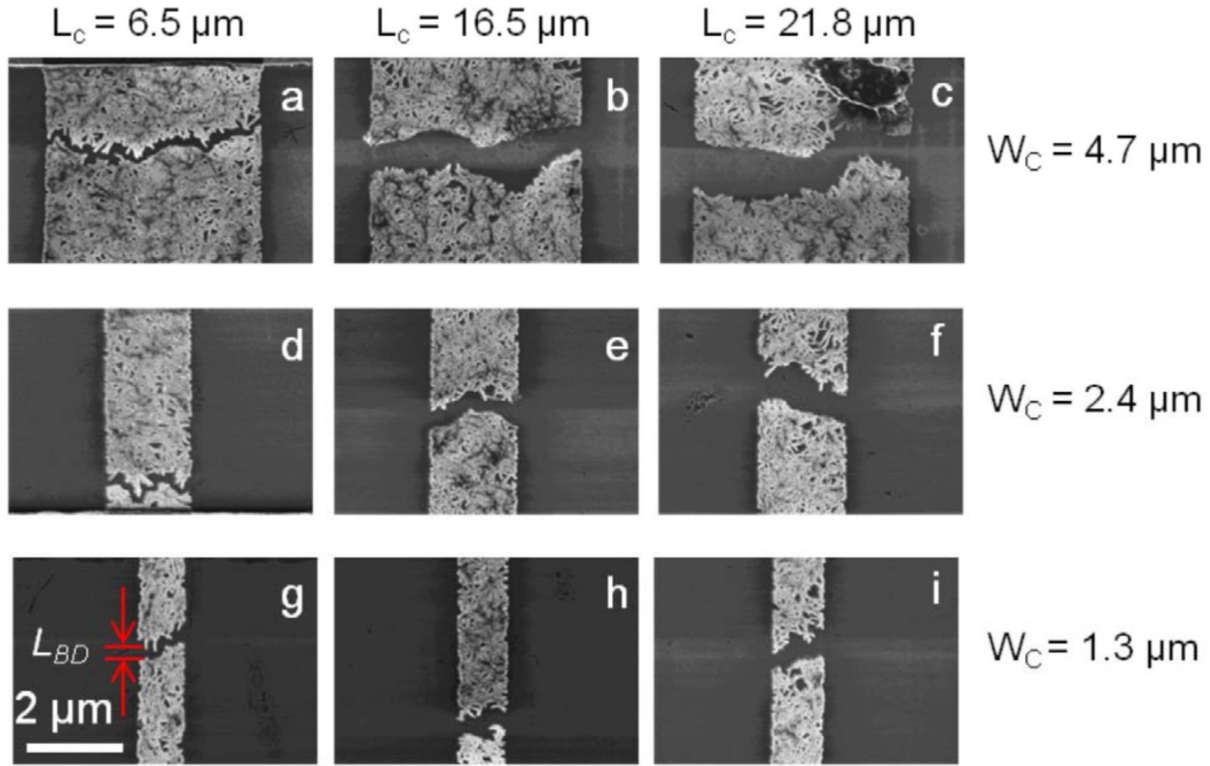

Figure 5. Scanning electron microscopy (SEM) images of CN-TFTs after complete breakdown for different channel lengths (L_C = 6.5 μm, 16.5 μm, 21.8 μm) and widths (W_C = 1.3 μm, 2.4 μm, 4.7 μm). The breakdown gap length (L_{BD}) in the CN-TFT increases as the L_C is increased; however L_{BD} does not show much variation when the width is changed.

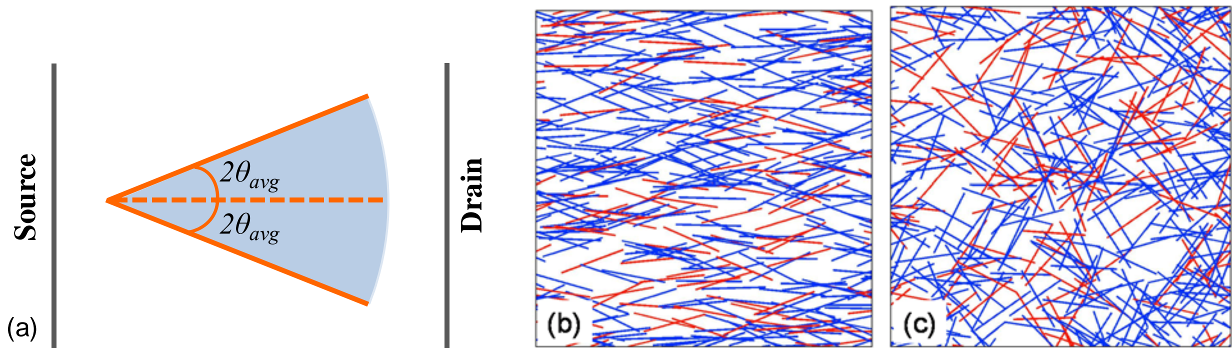

Figure 6. (a) The schematic illustrates the alignment of a CNT. The average alignment (θ_{avg}) of the CNT network is defined such that for a specific value of θ_{avg}, a CNT in the network is allowed to make any angle between $-2\theta_{avg}$ and $2\theta_{avg}$ with equal probability. Hence, by this definition, $\theta_{avg} = 45°$ corresponds to a random network, and $\theta_{avg} = 0°$ means perfectly aligned CNTs. A example of heterogeneous CNT network with (b) $\theta_{avg} = 13°$; (c) $\theta_{avg} = 36°$. Metallic (M) CNTs in brown, semiconducting (S) CNTs in blue; M:S network density ratio is 1:2.

This is an author-produced, peer-reviewed version of this article. The final, definitive version of this document can be found online at *Nanotechnology*, published by Institute of Physics. Copyright restrictions may apply. DOI: 10.1088/0957-4484/24/40/405204.

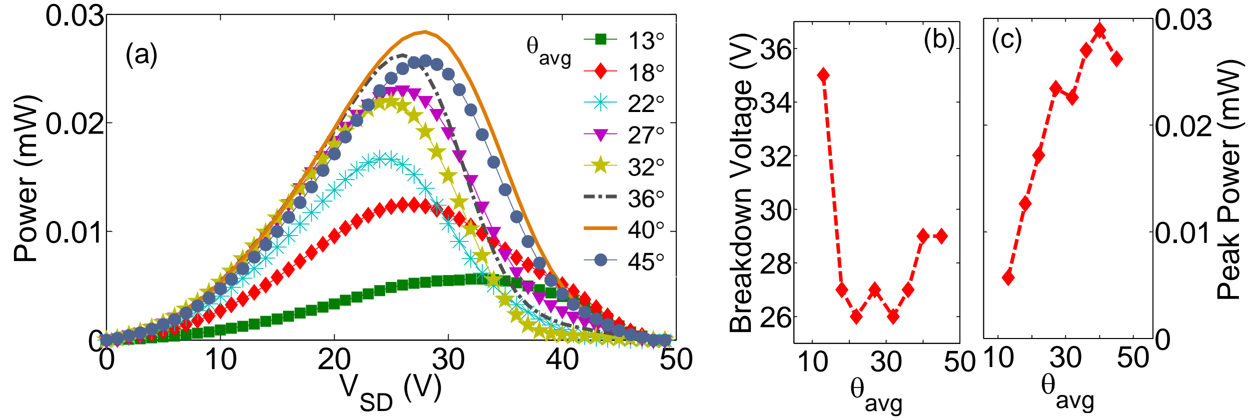

Figure 7. (a) Power dissipation vs. source-to-drain voltage (V_{SD}) for different alignments (θ_{avg}) of CNTs in the network. (b, c) V_{BD} and P_{BD} vs. θ_{avg} respectively. Here, $L_t = 2$ µm, $L_C = 10$um, $W_C = 10$ µm, ρ = 15 CNTs/µm^2. Metallic to semiconducting CNT ratio in the network is 1:2 and their electrical conductivity ratio is 5:1. It should be noted that very few (< 10%) devices have connected pathways at very low angle ($\theta_{avg} < 10°$). However, this number improves (e.g. >70% for $\theta_{avg} = 13°$) significantly for higher θ_{avg}.

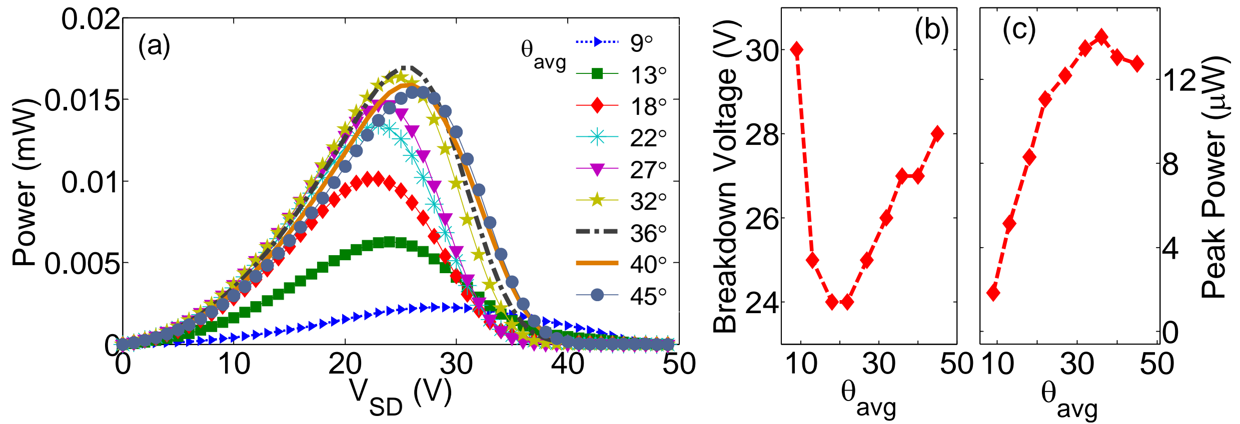

Figure 8. (a) Plot of power dissipation in the device vs. source-to-drain voltage (V_{SD}) for different alignments (θ_{avg}) of CNTs of purely semiconducting network. (b), (c) breakdown voltage (V_{BD}) and peak power (P_{BD}) are plotted vs. θ_{avg}. Here $L_t = 2$ µm, $L_C = 10$ µm, $W_C = 10$ µm, and $\rho = 15$ CNTs/µm^2.

This is an author-produced, peer-reviewed version of this article. The final, definitive version of this document can be found online at *Nanotechnology*, published by Institute of Physics. Copyright restrictions may apply. DOI: 10.1088/0957-4484/24/40/405204.

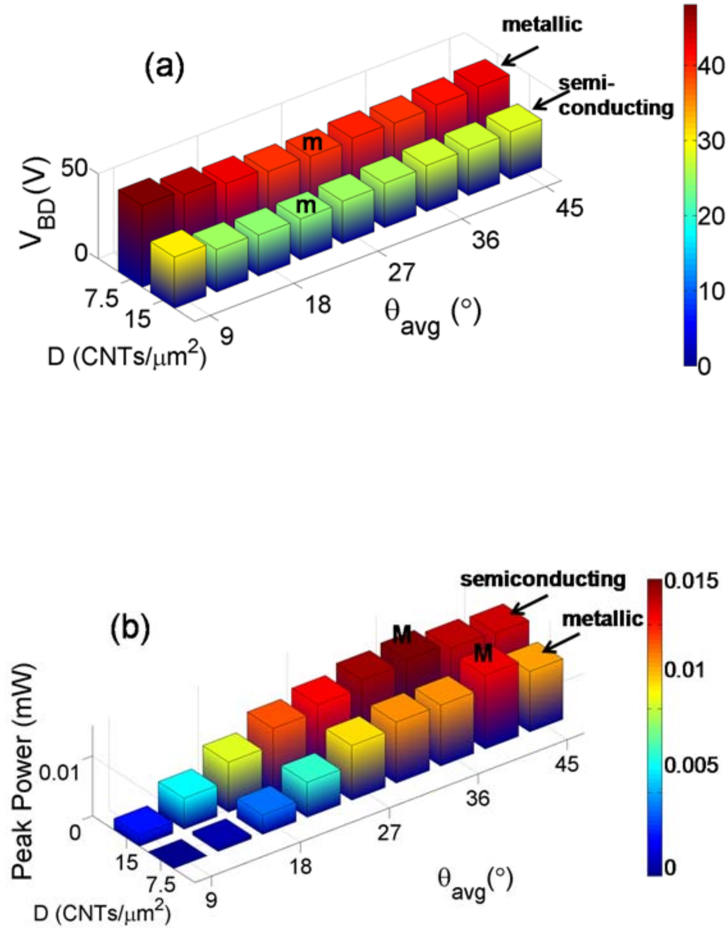

Figure 9. A bar plot of (a) breakdown voltage (V_{BD}), (b) peak power dissipation (P_{BD}) versus network alignment (θ_{avg}) for metallic (ρ = 7.5 CNTs/μm^2) and semiconducting (ρ = 15 CNTs/μm^2) networks. Letters 'm' and 'M' denote the location of minima and maxima respectively. The metallic to semiconducting CNT density ratio is 1:2 which is same as that in typical unsorted CNT network.

This is an author-produced, peer-reviewed version of this article. The final, definitive version of this document can be found online at *Nanotechnology*, published by Institute of Physics. Copyright restrictions may apply. DOI: 10.1088/0957-4484/24/40/405204.

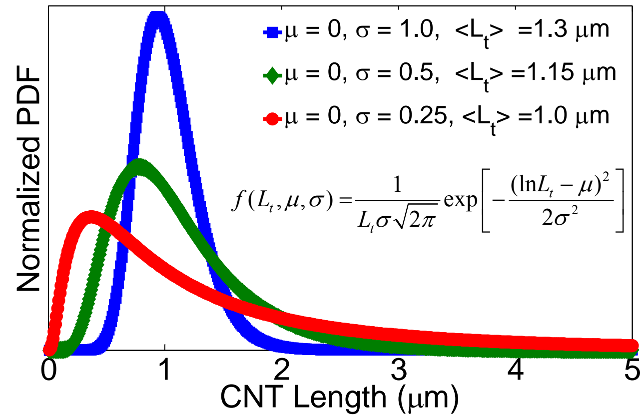

Figure 10. Three different log-normal CNT length distributions in the network with average CNT length, $<L_t> = 1$ μm, 1.15 μm and 1.3 μm.

This is an author-produced, peer-reviewed version of this article. The final, definitive version of this document can be found online at *Nanotechnology*, published by Institute of Physics. Copyright restrictions may apply. DOI: 10.1088/0957-4484/24/40/405204.

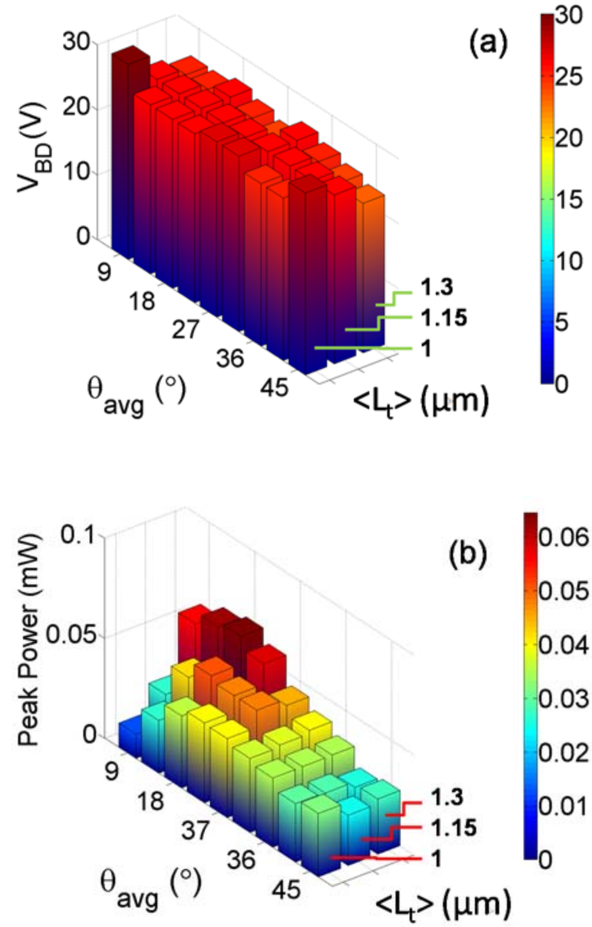

Figure 11. A bar plot of (a) breakdown voltage (V_{BD}) (b) peak power (P_{BD}) for different alignment and length distributions of the CNT network. The V_{BD} shows little variation as alignment or length distribution is changed, whereas the P_{BD} shows a strong correlation with alignment; this correlation changes significantly as length distribution is changed.

This is an author-produced, peer-reviewed version of this article. The final, definitive version of this document can be found online at *Nanotechnology*, published by Institute of Physics. Copyright restrictions may apply. DOI: 10.1088/0957-4484/24/40/405204.

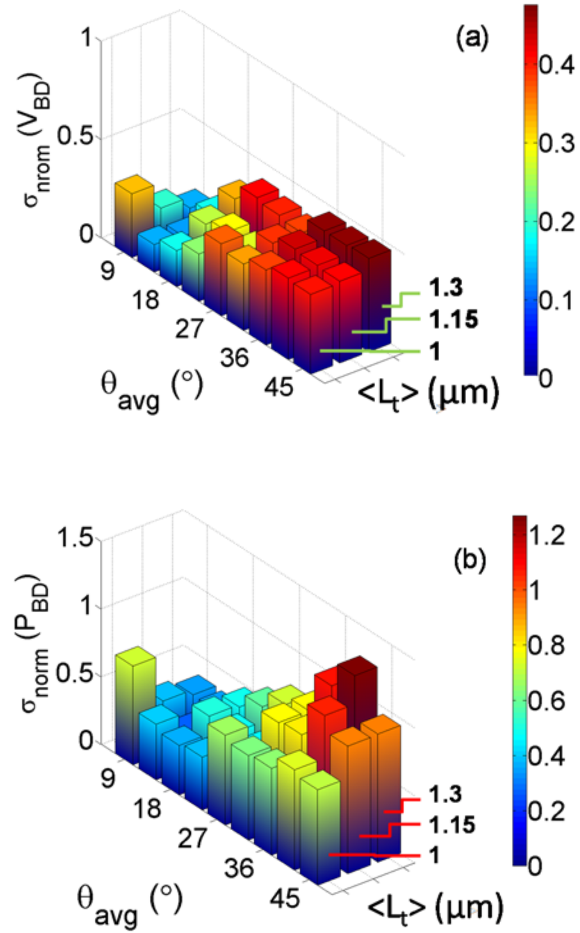

Figure 12. A bar plot of normalized standard deviation (σ_{norm}) of (a) breakdown voltage (V_{BD}), (b) peak power (P_{BD}) for different alignment and length distributions of the CNT network.

This is an author-produced, peer-reviewed version of this article. The final, definitive version of this document can be found online at *Nanotechnology*, published by Institute of Physics. Copyright restrictions may apply. DOI: 10.1088/0957-4484/24/40/405204.

Supporting Information

Table of Parameters used in Electro-Thermal Model

Variable	Name	Nominal Value
$\xi = (T-T_\infty)/(Q' dL_t/k_t)$	Non-dimensional Temperature	-
T	Temperature	(Kelvin)
T_∞	Ambient Temperature	298 K
d	Diameter	2 nm
L_t	CNT length	2 µm
k_t	Thermal conductivity of CNT	1000 W/mK
k_{OX}	Thermal conductivity of oxide	1 W/mK
t_{OX}	Oxide thickness	300 nm
t_{Si}	Si thickness	500 µm
$\tilde{G}_S$	Non-dimensional thermal conductance at CNT-oxide interface	2 x 10^{-4}
$\tilde{G}_C$	Non-dimensional thermal conductance at CNT-CNT junction	10^{-7}
C_{ij}	Charge transfer coefficient	50

This is an author-produced, peer-reviewed version of this article. The final, definitive version of this document can be found online at *Nanotechnology*, published by Institute of Physics. Copyright restrictions may apply. DOI: 10.1088/0957-4484/24/40/405204.

S1. Breakdown Characteristics from Experimental Results

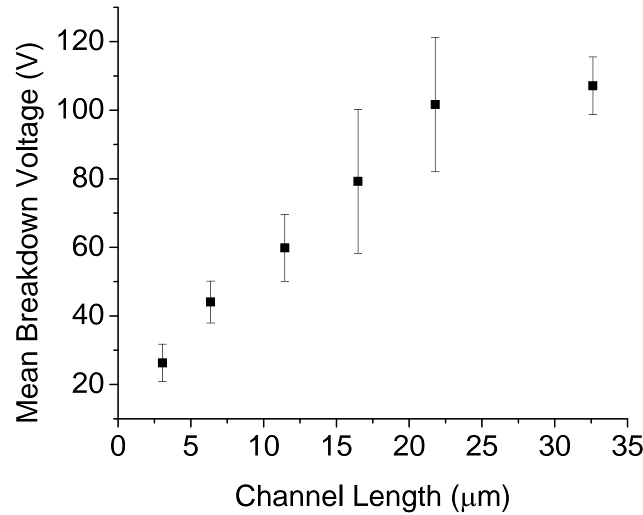

Figure S-1 Variation of the breakdown voltage V_{BD} versus channel length (L_C). Experimental results are obtained for limited number of devices (total ~30 devices including all the cases). Nevertheless, the general trend agrees well with the simulation results.

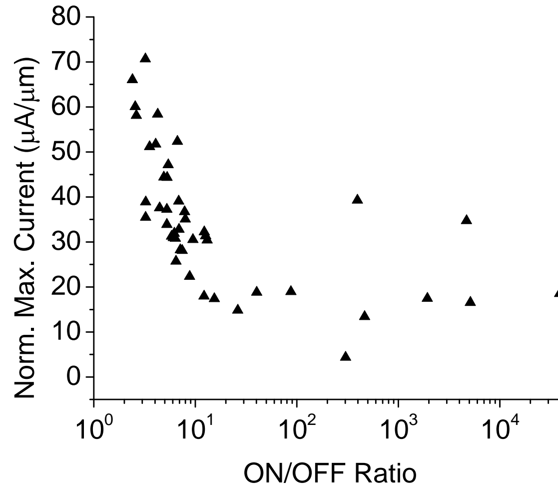

Figure S-2 Variation of normalized maximum current (normalized with respect to *W*) versus ON/OFF ratio of CN-TFTs. For devices with higher ON/OFF ratio, the maximum current density before breakdown is observed to be lower compared to the devices with lower ON/OFF ratio. We observed that for semiconducting networks the maximum current is usually lower than the metallic network. Therefore, narrow networks which have more semiconducting paths show lower current capacity. It should be noted that such dependence is observed only when *W* is less than or comparable to average CNT length and does not exist in case of larger *W*.

This is an author-produced, peer-reviewed version of this article. The final, definitive version of this document can be found online at *Nanotechnology*, published by Institute of Physics. Copyright restrictions may apply. DOI: 10.1088/0957-4484/24/40/405204.

S2. Breakdown Behavior for Different Orientation Distributions and Lognormal CNT Length Distributions

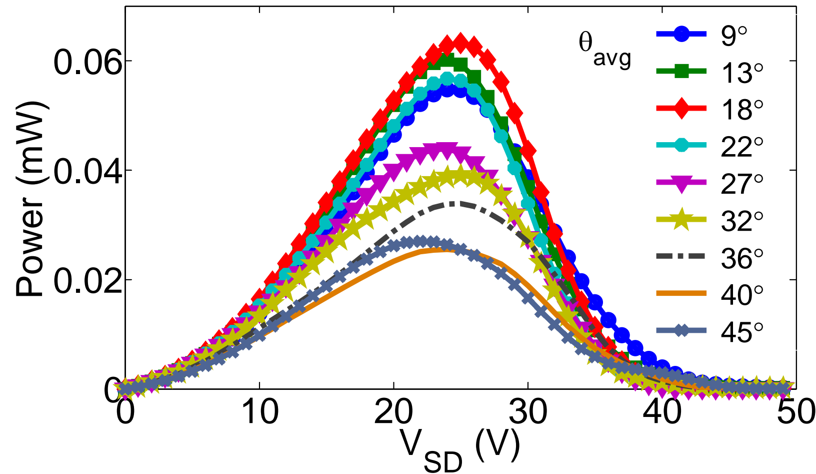

Figure S-3. Variation in power dissipation with source-to-drain voltage for several alignment cases; CNT length distribution corresponds to μ = 0, σ = 1 and average CNT length = 1.3 μm. Maximum power dissipation increases with θ_{avg} for θ_{avg} = 9° to 18°, however it decreases significantly for further increase in θ_{avg}, i.e., the maximum power dissipation is highest for θ_{avg} = 18°. It can be noted that the random network (θ_{avg} = 45°) shows the poorest performance from the point of breakdown behavior and thermal reliability. Interestingly, the voltage corresponding to the peak power does not vary much as θ_{avg} is changed despite the fact that peak power can change upto three times in the range of θ_{avg} considered.

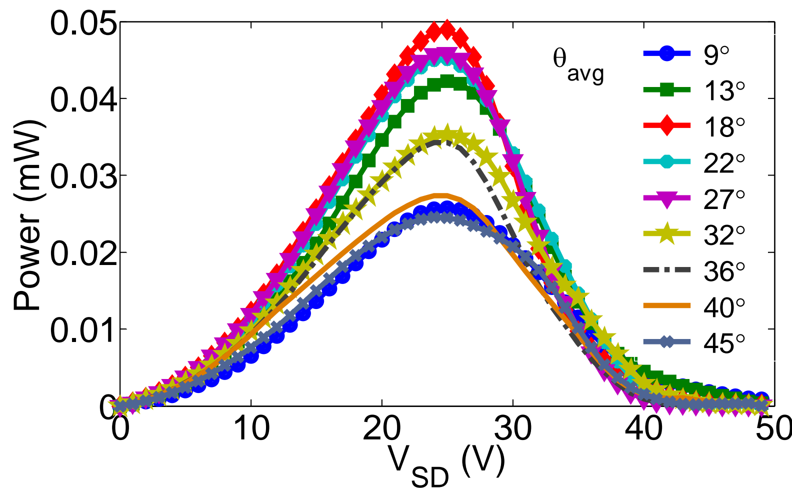

Figure S-4. Variation in power dissipation with source-to-drain voltage for several alignmentcases; CNT length distribution corresponds to μ = 0, σ = 0.5 and average CNT length = 1.15 μm. Maximum power dissipation is highest for θ_{avg} = 18°. It can be noted here that both highly aligned (θ_{avg} = 9°) and random network (θ_{avg} = 45°) show the poorest performance from the point of breakdown behavior and thermal reliability.

This is an author-produced, peer-reviewed version of this article. The final, definitive version of this document can be found online at *Nanotechnology*, published by Institute of Physics. Copyright restrictions may apply. DOI: 10.1088/0957-4484/24/40/405204.

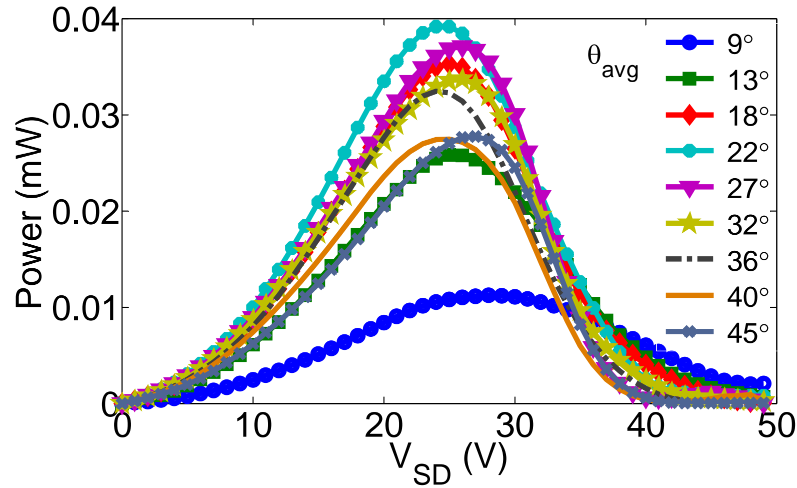

Figure S-5. Variation in power dissipation with source-to-drain voltage for several alignment cases; CNT length distribution corresponds to μ = 0, σ = 0.25 and average CNT length = 1 μm. Maximum power dissipation is highest for θ_{avg} = 22°. It can be noted here that the highly aligned network (θ_{avg} = 9°) shows the poorest performance from the point of breakdown behavior and thermal reliability. Also, the difference in the highest maximum power dissipation (at θ_{avg} = 22°) and maximum power dissipation of random network (θ_{avg} = 45°) is significantly less compared to previous two cases (see Figs. S3 and S4). This trend is very similar to that obtained for constant CNT length case since the lognormal CNT length distribtion for this case closely resembles to constant CNT length case.